The International Journal of Advanced Manufacturing Technology (2019) 101:1143–1156
https://doi.org/10.1007/s00170-018-3012-8

ORIGINAL ARTICLE

Improvements of machinability of aerospace-grade Inconel alloys with ultrasonically assisted hybrid machining

Wei Bai[1,2] · Anuj Bisht[3] · Anish Roy[2] · Satyam Suwas[3] · Ronglei Sun[1] · Vadim V. Silberschmidt[2]

Received: 9 April 2018 / Accepted: 6 November 2018 / Published online: 14 November 2018

Abstract

Aerospace-grade Ni-based alloys such as Inconel 718 and 625 are widely used in the airspace industry thanks to their excellent mechanical properties at high temperatures. However, these materials are classified as 'difficult-to-machine' because of their high shear strength, low thermal conductivity, tendency to work-harden and presence of carbide particles in their microstructure, which lead to rapid tool wear. Machining-induced residual stresses in a machined part is an important parameter which is assessed since it can be used to evaluate overall structural resilience of the component and its propensity to fatigue failure in-service. Ultrasonically assisted turning (UAT) is a hybrid machining technique, in which tool-workpiece contact conditions are altered by imposing ultrasonic vibration (typical frequency ~ 20 kHz) on a tool's movement in a cutting process. Several studies demonstrated successfully the resulting improvements in cutting forces and surface topography. However, a thorough study of UAT-induced residual stresses is missing. In this study, experimental results are presented for machining Inconel 718 and 625 using both conventional turning (CT) and UAT with different machining parameters to investigate the effect on cutting forces, surface roughness and residual stresses in the machined parts. The study indicates that UAT leads to significant cutting force reductions and improved surface roughness in comparison to CT for cutting speeds below a critical level. The residual stresses in machined workpiece show that UAT generates more compressive stresses when compared to those in CT. Thus, UAT demonstrates an overall improvement in machinability of Inconel alloys.

Keywords Ultrasonically assisted turning · Machinability · Residual stress · Structural integrity · Inconel alloys

1 Introduction

As heat-resistant superalloys, Inconel alloys are extensively used in the aerospace industry for components exposed to harsh environments, such as in critical parts of gas turbine engines, nuclear power plants and pressure vessels. Inconel alloys have excellent strength properties (up to 650 °C), low thermal conductivity and corrosion resistance [1]. However, these very properties are responsible for Inconel's poor machinability characteristics [2]. Low thermal conductivity leads to high cutting temperatures in a process zone, imposing steep temperature gradients in the tool. Nickel-based superalloys also demonstrate high chemical affinity to many tool materials exacerbating tool wear. In addition, Inconel is sensitive to strain rate and work hardens rapidly, causing abrasive wear, particularly at the tool's tip and leading-edge positions. As a result, high temperature in the process zone and severe tool wear generate poor surface quality.

Assessing structural integrity of parts is essential for reliability analysis. Machining studies showed that the residual-stress profile was typically tensile in nature at a machined workpiece surface [3]. Outeiro et al. [4] and Wardany et al. [5] reported that thermal loads promoted tensile stresses, with mechanical loads being responsible for compressive residual stresses. In general, compressive residual stresses are beneficial to service life of components, whereas tensile ones are detrimental [6]. Optimum machining conditions were also

✉ Ronglei Sun
ronglei@hust.edu.cn

✉ Vadim V. Silberschmidt
v.silberschmidt@lboro.ac.uk

[1] The State Key Laboratory of Digital Manufacturing Equipment and Technology, School of Mechanical Science and Engineering, Huazhong University of Science and Technology, Wuhan 430074, China

[2] Wolfson School of Mechanical, Electrical and Manufacturing Engineering, Loughborough University, Leicestershire LE11 3TU, UK

[3] Department of Materials Engineering, Indian Institute of Science, Bangalore 560 012, India

studied to achieve compressive surface residual stresses or minimal tensile residual stresses [7, 8]. Besides, in cutting of difficult-to-machine materials, consumption of cooling lubricant is a significant problem. It substantially increases the total process costs because of environmental concerns: the associated costs from coolant acquisition to its disposal are almost four times higher than those of consumable tooling [9]. Thus, dry machining is the meaningful way to reduce the manufacturing costs and make the processes environmentally friendly. Meanwhile, achieving a high quality of finished components with dry machining is a well-known challenge.

Ultrasonically assisted turning (UAT) is a novel and effective hybrid machining technique for difficult-to-machine materials such as titanium [10] and nickel [11] alloys. Thanks to the periodic separation of a tool from a workpiece with ultrasonic frequency, thermomechanical behaviours of workpieces in UAT differ significantly from those in conventional turning (CT). Thus, UAT is regarded as a technique with a potential to improve the machinability of high-strength alloys. Prior studies indicated that UAT led to a reduction in cutting forces, improved surface roughness, with enhanced dynamical stability and tool life. Maurotto et al. [10] measured cutting force components at various process parameters in CT and UAT of β-titanium alloy, but the reason of forces reduction in ultrasonic vibration was not discussed. Mitrofanov et al. [12] developed the FE model of UAT to investigate the influence of lubrication and cutting parameters on the UAT process of Inconel 718. They concluded that the friction force at the tool-chip interface affected a maximum magnitude of the cutting force, and tool-chip disengagement in a vibration period reduced the level of average cutting forces in UAT. But research on cutting forces in UAT for a variety of nickel-based alloys and under different processing parameters was lacking. Babitsky et al. [11] measured surface roughness R_a and roundness of machined workpiece in CT and UAT of Inconel 718, and obtained nearly 50% reduction of surface roughness and 40% improvement of roundness in UAT. They explained that multiple-impact high-frequency interaction between a cutting tool and a chip due to applied ultrasonic vibration changed the material deformation processes and friction forces and increased dynamic stiffness of a lathe-tool-workpiece system. However, surface quality of various aerospace-grade Ni-based alloys with different material properties in UAT was not discussed.

Nath et al. [13, 14] studied tool wear using CBN and PCD tools in UAT of Inconel 718, and they found that UAT reduced tool wear by successive vibration impacts between the tool and workpiece. Other researchers also investigated some aspects of machinability of difficult-to-machine materials with ultrasonic vibration. However, only a few researchers investigated residual stresses of components machined with UAT. Sharma and Pandey [15] reported residual stresses in UAT of 4340 hardened steel for various machining and vibration parameters. The study showed that more compressive residual stresses could be generated by increasing the ultrasonic power during machining. Nestler and Schubert [16] studied surface properties for UAT of particle-reinforced aluminium matrix composites. They reported that higher compressive residual stresses were produced with UAT in both radial and cutting directions. Ahmed et al. [17] investigated hardness and residual stresses in machined surface for UAT of Inconel 718. Nanoindentation analysis demonstrated that the level of hardness of the surface layer in UAT was lower than that in CT and close to the hardness of the as-delivered material, which was also validated by Bai et al. [18]. However, they reported that the residual stresses in UAT were higher in comparison to those in CT. No other experimental investigations of residual stresses in UAT were carried for Inconel alloys to-date apart for [17] with only one machining condition.

As discussed, Inconel alloys are widely used in high-performance components under severe service conditions. Their poor machinability limits their application and affects the quality of processed parts. So, the aim of this paper is to study the feasibility of improving the machinability of nickel-based alloys by employing a hybrid machining process—UAT, and compare its effect on the machinability of two nickel-based alloys under different machining parameters together with resultant residual stresses.

In this study, the experimental analysis of machinability for UAT and CT of Inconel 718 and 625 is carried out. Section 2 describes the experimental work, including details of the setup and tools used, workpiece properties and experimental methodology. Experimental results such as cutting forces, surface topography and residual stresses are discussed in Section 3. The paper ends with some concluding remarks in Section 4.

2 Experimental work

2.1 Experimental setup

All experiments were performed on a modified lathe with an ultrasonic machining attachment. The system has the flexibility to switch between UAT and CT by turning an ultrasonic generator on or off. Figure 1 shows the experimental setup, a schematic of the ultrasonic cutting device and the coordinate system used to define kinematics of the machining process. Its ultrasonic generator applies electrical energy to a piezoelectric transducer, in which the piezo-ceramic rings generate axial vibration. This high-frequency low-amplitude mechanical vibration is transmitted to a tool via a tool-holder fixed to a horn/concentrator (Fig. 1b). The flange in the ultrasonic machining device is connected to a Kistler dynamometer with a fixture (Fig. 1a). The dynamometer is fixed on a feed platform via a pillar to make sure that the ultrasonic machining device moves synchronously with the feed system. The x, y and z

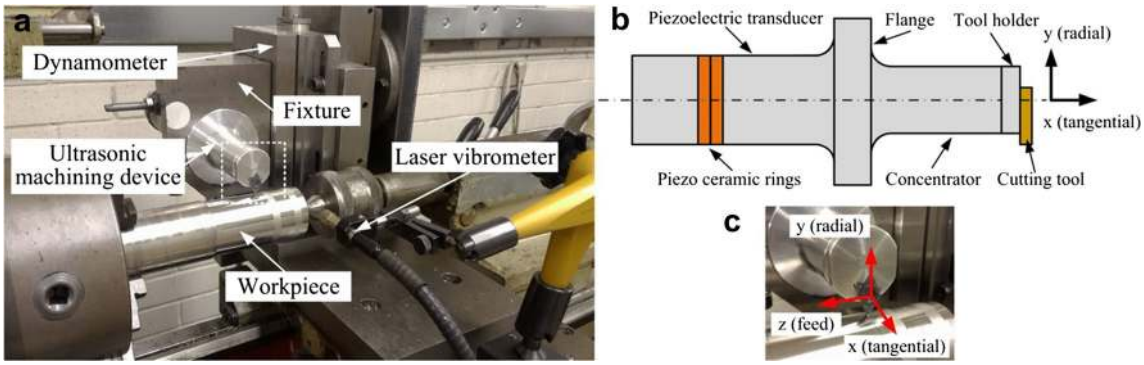

Fig. 1 Experimental setup: **a** ultrasonic cutting assembly, **b** schematic of ultrasonic machining device, **c** axes of cutting tool's movements

axes represent the main cutting direction (referred to as tangential direction), radial direction and feed direction, respectively (Fig. 1c). Note that ultrasonic vibration was imposed in the tangential direction in the presented tests.

2.2 Machine tool and machining conditions

A coated cemented-carbide tool (DCMT 11T304-MF1105) was used in all the experiments; its details are presented in Table 1.

For the UAT process, a critical velocity of a cutting tool for tool-workpiece separation can be expressed as [11]:

$$V_c = 2\pi fA, \tag{1}$$

where f (kHz) is the vibration frequency and A (μm) is the vibration amplitude. As an example, for most experiments carried out in this study, the vibration frequency f and peak-to-peak amplitude ($2A$) were 18.11 kHz and 8.4 μm, respectively. Thus, the critical velocity V_c was calculated to be 28.7 m/min, implying effectiveness of ultrasonic machining at cutting speeds below this threshold. Any speed above this limit essentially reduces UAT to a CT process.

Several experiments were carried out by varying the levels of cutting speed, feed rate, depth of cut and vibration amplitude as listed in Table 2.

Table 1 Cutting tool specification

Tool maker	SANDVIK
Tool number	DCMT 11T304-MF1105
Tool material	Tungsten carbide
Coating	TiAlN
Nose radius (mm)	0.397
Rake angle (°)	0
Clearance angle (°)	7

2.3 Workpiece material

In this study, round ingots of Inconel 718 and 625 were machined, which are high-strength, corrosion-resistant nickel-chromium superalloys; the compositions of the materials are shown in Table 3.

These nickel-chromium superalloys have similar composition, with higher contents of Fe in Inconel 718 and Mo in Inconel 625. Both alloys exhibit precipitation of intermetallic phases and carbides. Studies of microstructure and phases were carried out for Inconel 718. Figure 2a shows precipitates after solution annealing at a low temperature of 954 °C for 1 hour and water quenching, which yielded hardness of 22 HRC. A δ phase was present along the grain boundaries, and with black globular particles are MC carbides. Figure 2b presents the equiaxed grains of the γ phase, crystal orientation and inverse-pole-figure colouring obtained with EBSD.

Nominal mechanical properties of solution-annealed Inconel 718 and 625 are listed in Table 4. The two alloys show close properties except for measured tensile and shear strengths (with Inconel 718 outperforming Inconel 625) as well as elongation to failure, which is expected to influence machinability of these alloys.

Table 2 Cutting conditions of turning experiments

Exp. No	Cutting speed (m/min)	Feed rate (mm/rev)	Depth of cut (mm)	Vibration amplitude, peak-to-peak (μm)
1	20	0.08	0.12	8.4
2	30			
3	40			
4	20	0.16		
5		0.25		
6		0.08	0.20	
7			0.28	
8			0.12	6.7
9				4.9

Table 3 Chemical composition of workpiece materials

Inconel 718	Ni	Cr	Fe	Nb + Ta	Mo	Ti	Al	Co	Si	Mn
	54	17.84	18.37	5.11	2.9	0.96	0.53	0.09	0.07	0.05
Inconel 625	Ni	Cr	Mo	Fe	Nb + Ta	Ti	Al	Si	Co	Mn
	58	22.1	9.1	4.73	3.4	0.33	0.21	0.1	0.08	0.11

2.4 Experimental methodology

In this study, the cutting forces, surface topology and residual stress of the machined surface by CT and UAT were investigated. Detailed results of the measurements made are presented in this section.

2.4.1 Cutting force measurements

A three-component Kistler dynamometer (type 9257B) was employed to measure the cutting forces; it was connected to the ultrasonic machining device as shown in Fig. 1. The dynamometer can measure a maximum force of 5 kN with a natural frequency of 3.5 kHz. Three orthogonal components of a force in the x, y and z directions corresponding to the tangential, radial and feed directions, provided data for the primary cutting force, thrust force and feed force during machining. An electrical signal from the dynamometer was amplified by a Kislter charge amplifier (type 5015A). The obtained signals were processed and visualised using a PicoScope 4224 high-resolution oscilloscope.

2.4.2 Surface topography measurement

To obtain the surface topography, an optical 3D measurement device (Alicona Infinite Focus G4) was utilised to assess the surfaces machined with CT and UAT; dimensions of a sampling area were 1 mm × 1.2 mm. Results for the surface profile, roughness and topography of samples obtained with the two studied machining techniques are presented in Section 3.

2.4.3 Residual-stress measurements

A uniaxial residual stress on the surface of as-turned samples (both for CT and UAT) was measured using an X-ray-diffraction-based technique. The measurements were carried out with Bruker D8 Discover using Co Kα radiation operating at 40 kV and 40 mA. A $\sin^2\psi$ method was used for calculation of the uniaxial residual stress [19, 20]. An X-ray diffraction-peak profile corresponding to the (111) crystallographic plane was recorded at six different ψ values ranging from 0 to 45°. The plane was selected as the intensity of other higher-order hkl planes was not significant during the measurement. A step size of 0.01° and a time interval of 2 s/step were used. A sample was positioned during the measurement so that to obtain the resultant residual value along the axial direction of the turned workpiece. After the measurement, the uniaxial residual stress was calculated using the following equation [19, 20]:

$$\sigma_\varphi = \frac{E}{(1+\nu)\sin^2\psi}\left(\frac{d_\psi - d_n}{d_n}\right), \tag{2}$$

where E (GPa) is the elastic modulus, ν is the Poisson's ratio of 0.294, d_ψ (Å) is the inter-planar spacing at a particular angle ψ (deg), d_n (Å) is the inter-planar spacing at normal incidence ($\psi = 0^\circ$).

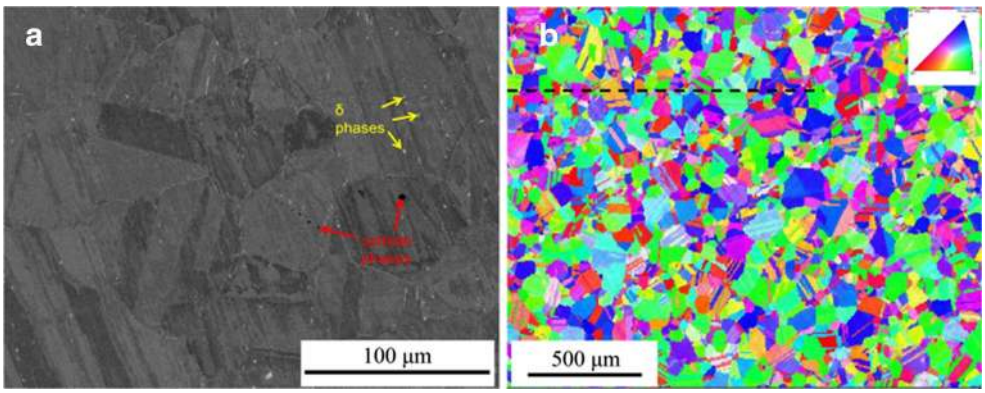

Fig. 2 Microstructural analysis of Inconel 718: **a** optical microscopy, **b** EBSD

Table 4 Mechanical properties of workpiece materials

Workpiece material	Inconel 718	Inconel 625
Producer	ATI Specially Materials Ltd.	
Heat treatment	Solution annealed	
Workpiece diameter, D (mm)	50	50
Young's modulus, E (GPa)	190	200
Tensile strength UTS (MPa)	1200	880
Shear strength (MPa)	660~950	530~600
Elongation (%)	12–19	33–36
Density, ρ (kg/m^3)	8220	8600
Melting point, (°C)	1260	1290
Specific heat, (J/kg K)	450	440
Thermal conductivity, k (W/m K)	11.4	9.8

3 Results and discussion

3.1 Cutting forces

The measured levels of cutting forces were compared for CT and UAT performed with various machining parameters for the two alloys (Fig. 3). Application of ultrasonic vibration led to a significant reduction in cutting forces, especially for the tangential force component. For a cutting speed of 20 m/min, which was below the calculated critical speed of 28.7 m/min for a peak-to-peak amplitude of 8.4 μm, a noticeable reduction for all force components was observed (Fig. 3(a1, a2)). The cutting force in CT decreased with an increase in the cutting speed from 20 m/min to 40 m/min (Fig. 3(a1)). In contrast, the cutting force in UAT of Inconel 718 increased with an increase in the cutting speed from 20 m/min to 30 m/min, since higher speeds imply a longer tool contact time (less separation) for each vibratory cycle of the tool. Interestingly, a small yet non-negligible reduction in cutting forces was observed even when the cutting velocity exceeded the theoretical critical velocity threshold (Fig. 3(a1)). We believe that this was due to the reciprocating tool motion, where during the retraction stage, the effective velocity between the tool and the workpiece was lower than the nominal cutting velocity leading to an overall reduction in observed cutting forces. As a result of the discussed variation in material and mechanical properties of the two studied alloys, differences in force reductions were observed. The cutting forces in CT of Inconel 625 had a trend similar to that for Inconel 718 for cutting speed below than 30 m/min, as Devillez et al. [21] reported that the forces decreased with the cutting speed when turning Inconel alloy at feed rate of 0.1 mm/rev. However, the decline of the cutting force at higher cutting speed (40 m/min) for Inconel 718 was larger than that for Inconel 625. The reason was that a higher concentration of Fe in Inconel 718 diffused into the tool's binder (Co) causing severer wear than that in Inconel 625 [22]. Surface roughness of the machined surfaces in Section 3.2 also show higher R_a and R_q generate by CT in Inconel 718 (compared to Inconel 625), which means that is caused swifter tool wear at higher cutting speed than Inconel 625. Although the tool wear at various cutting stages affected force changes, the effective depth-of-cut reduced by wear when turning Inconel 718 for depth-of-cut (0.12 mm) comparable with the tool geometry (nose radius of 0.397 mm) resulted in higher forces reduction at higher cutting speed. The extent of force reduction with ultrasonic assistance decreased from 53% at 20 m/min to 22% at 30 m/min and 17% at 40 m/min for Inconel 718, in comparison to 52%, 31% and 21%, respectively, for Inconel 625.

Analysis of the effect of varying feed rate on the machining forces showed that the cutting and thrust forces in both CT and UAT for two alloys increased with an increase in the feed rate (Fig. 3(b1, b2)). However, the force reduction in UAT for Inconel 718 reduced from 53% at 0.08 mm/rev to 29% at 0.16 mm/rev and 18% at 0.25 mm/rev (Fig. 3(b1)). Similarly, force reduction for Inconel 625 reduced from 52 to 31% and 33% for similar feed rates, respectively (Fig. 3(b2)).

With an increase in the depth-of-cut, a similar trend for the cutting force was observed (Fig. 3(c)). The reduction of cutting force for greater depth of cut at 0.2 mm and 0.28 mm were only 25% and 28% for Inconel 718, respectively (Fig. 3(c1)). For Inconel 625, non-linear changes of the cutting force decline were also found with the increasing depth-of-cut; from 36% at 0.12 mm to 25% at 0.20 mm and 42% at 0.28 mm. This phenomenon of non-linear variation also appeared in surface roughness data (Fig. 7(c2)). The cutting forces in UAT with higher levels of feed rate (0.25 mm/rev) and depth-of-cut (0.28 mm) for Inconel 625 (Fig. 3(b2, c2)) showed larger reductions than those for Inconel 718 (Fig. 3(b1, c1)). This was due to the higher elongation and lower tensile/shear strength of Inconel 625 resulting in its stronger acoustic softening than that of Inconel 718.

The effect of varying vibration amplitude is shown in Fig. 3(d1, d2), where an amplitude of 0 μm represents the CT process. Apparently, a reduction of cutting forces increased with an increase in the imposed vibration amplitude for two alloys. There is an exception for an amplitude of 4.9 μm because of the critical speed is 16.7 m/min in that process, which was lower than the cutting speed (20 m/min).

In summary, an optimised set of machining parameters can be found, with the cutting speed below the critical speed, low feed rate and depth-of-cut with a large superimposed amplitude, to yield the highest force reductions in turning of two Inconel alloys.

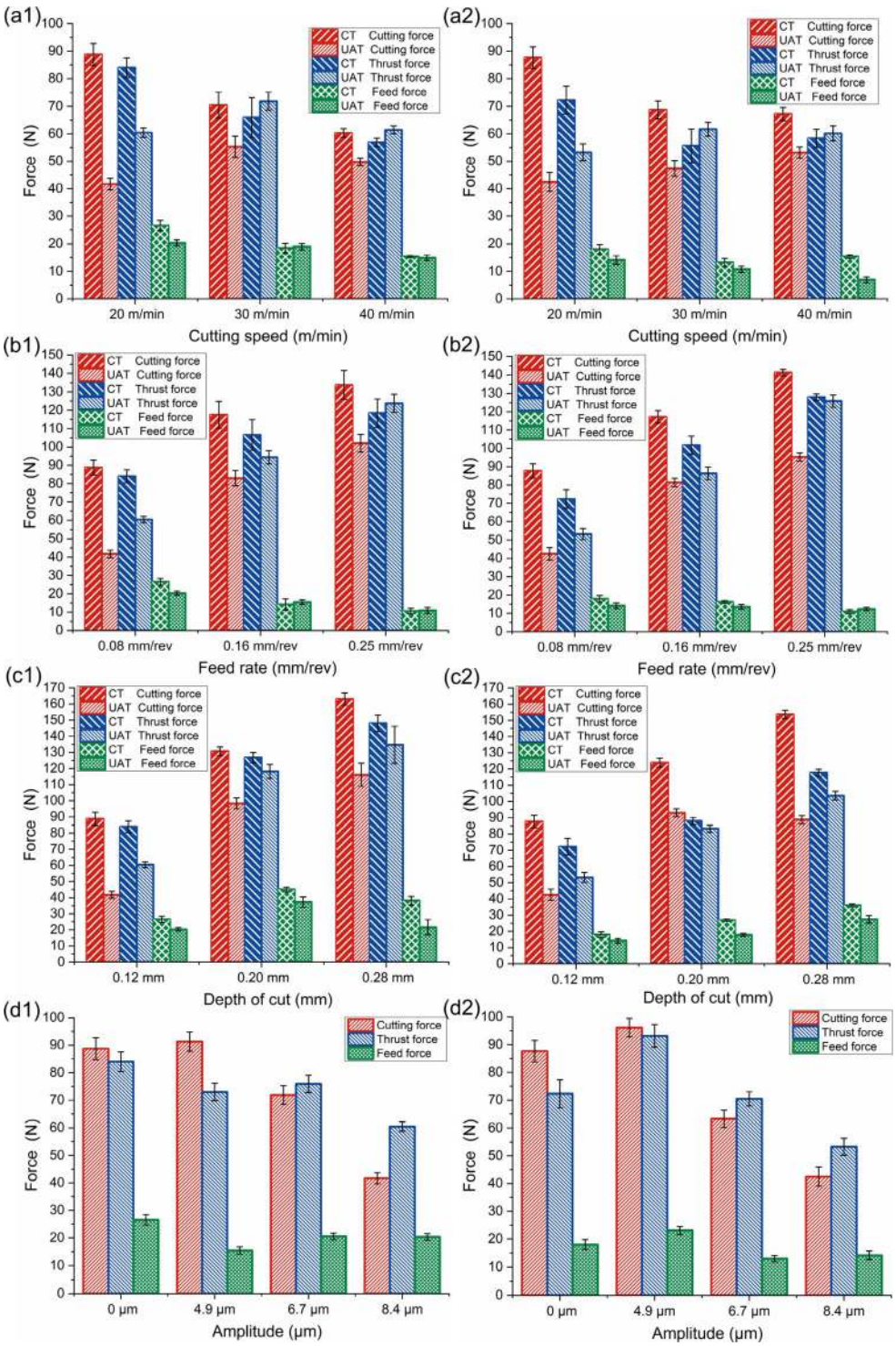

Fig. 3 Comparisons of average cutting forces in various cutting conditions by CT and UAT for Inconel 718 (1) and Inconel 625 (2): (a) varying cutting speed at feed rate of 0.08 mm/rev, depth-of-cut of 0.12 mm, vibration amplitude of 8.4 μm; (b) varying feed rate at cutting speed of 20 m/min, depth-of-cut of 0.12 mm, vibration amplitude of 8.4 μm; (c) varying depth of cut at cutting speed of 20 m/min, feed rate of 0.08 mm/rev, vibration amplitude of 8.4 μm; (d) varying vibration amplitude at cutting speed of 20 m/min, depth-of-cut of 0.12 mm, feed rate of 0.08 mm/rev

3.2 Surface topography

The machined surfaces of the two bars of Inconel alloys were produced under different machining conditions, with each section machined with the same parameters having a width of ~ 6 mm. The surface of machined specimens was observed with a non-contact optical surface topography measurement system (Alicona Infinite Focus G4) (Fig. 4).

3D topography on the machined surface corresponding to a rectangular area of 1000 μm × 1200 μm was analysed for the materials under study (Fig. 5). The surface profiles for CT and UAT of the two alloys were assessed in the feed direction for

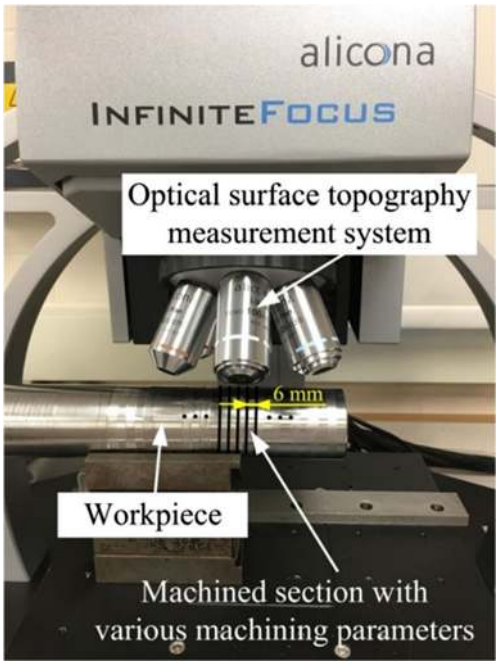

Fig. 4 Observation of topography of machined surface with optical measurement system

the following cutting conditions: a speed of 20 m/min, a feed rate of 0.08 mm/rev and a depth-of-cut of 0.12 mm. In UAT, vibration with an amplitude of 8.4 μm and a frequency of 18.11 kHz was imposed. Topography plots indicated that UAT produced significantly lower residual heights on the machined surface in both cutting and feed directions. In UAT, tool treads in the feed direction were present and micro-texture in the cutting direction appeared due to the alternating motion of the tool tip. In addition, in CT, the higher elongation of Inconel 625 led to more lateral flow of the workpiece material (Fig. 5(a2)) than that for Inconel 718 (Fig. 5(a1)).

In UAT, wider and deeper grooves appeared on the surface of in Inconel 625 (Fig. 5(b2)) than Inconel 718 (Fig. 5(b1)). As a result of a significantly improved surface roughness in UAT, the smooth surfaces of the workpieces appeared to have more shallow groves than in CT (the colour bars have the same scale in Fig. 5).

The surface profiles for CT and UAT of the two alloys were assessed for the same cutting conditions as used for the 3D topography test. The detailed results indicate that these

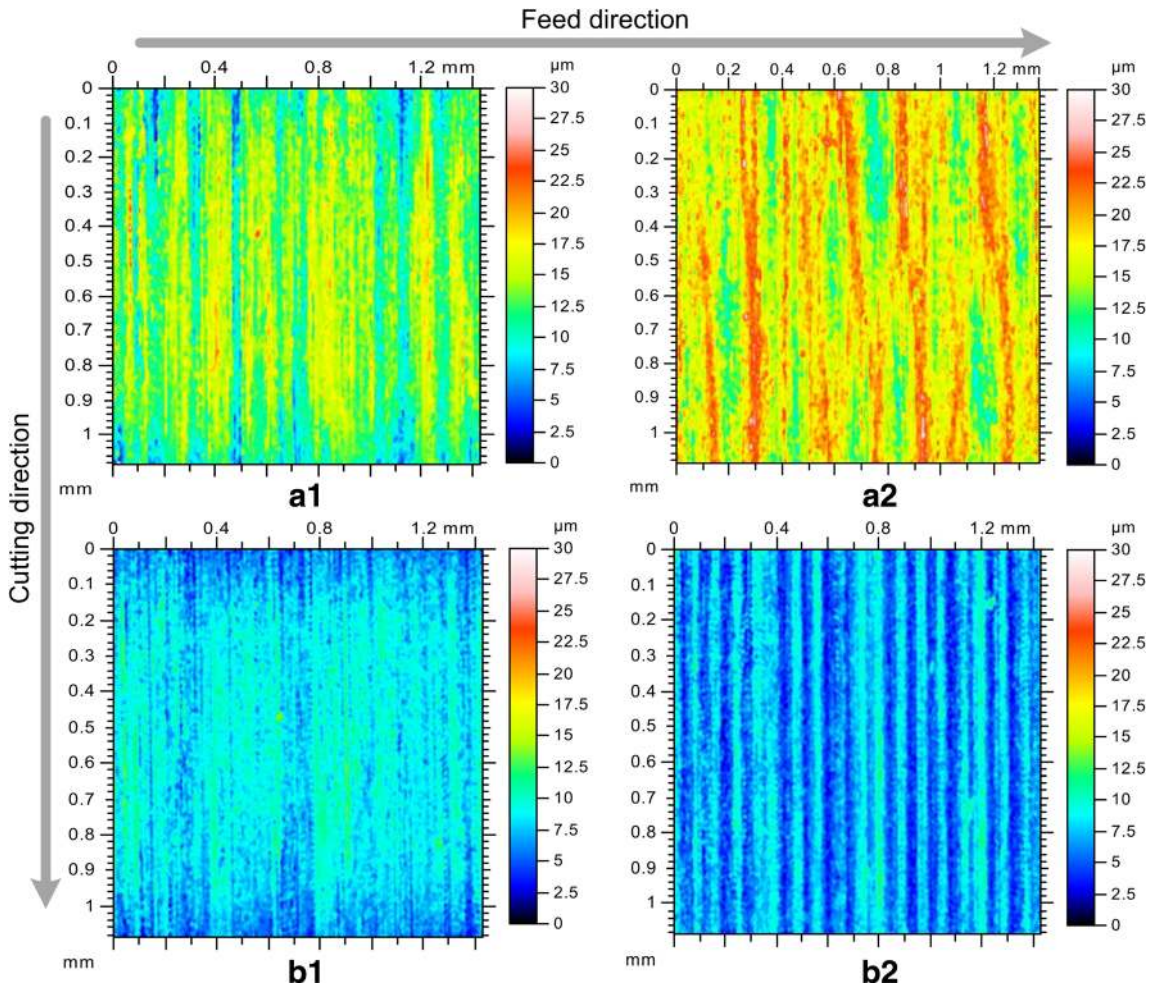

Fig. 5 Comparisons of surface topography: (a1) CT of Inconel 718; (a2) CT of Inconel 625; (b1) UAT of Inconel 718; (b2) UAT of Inconel 625

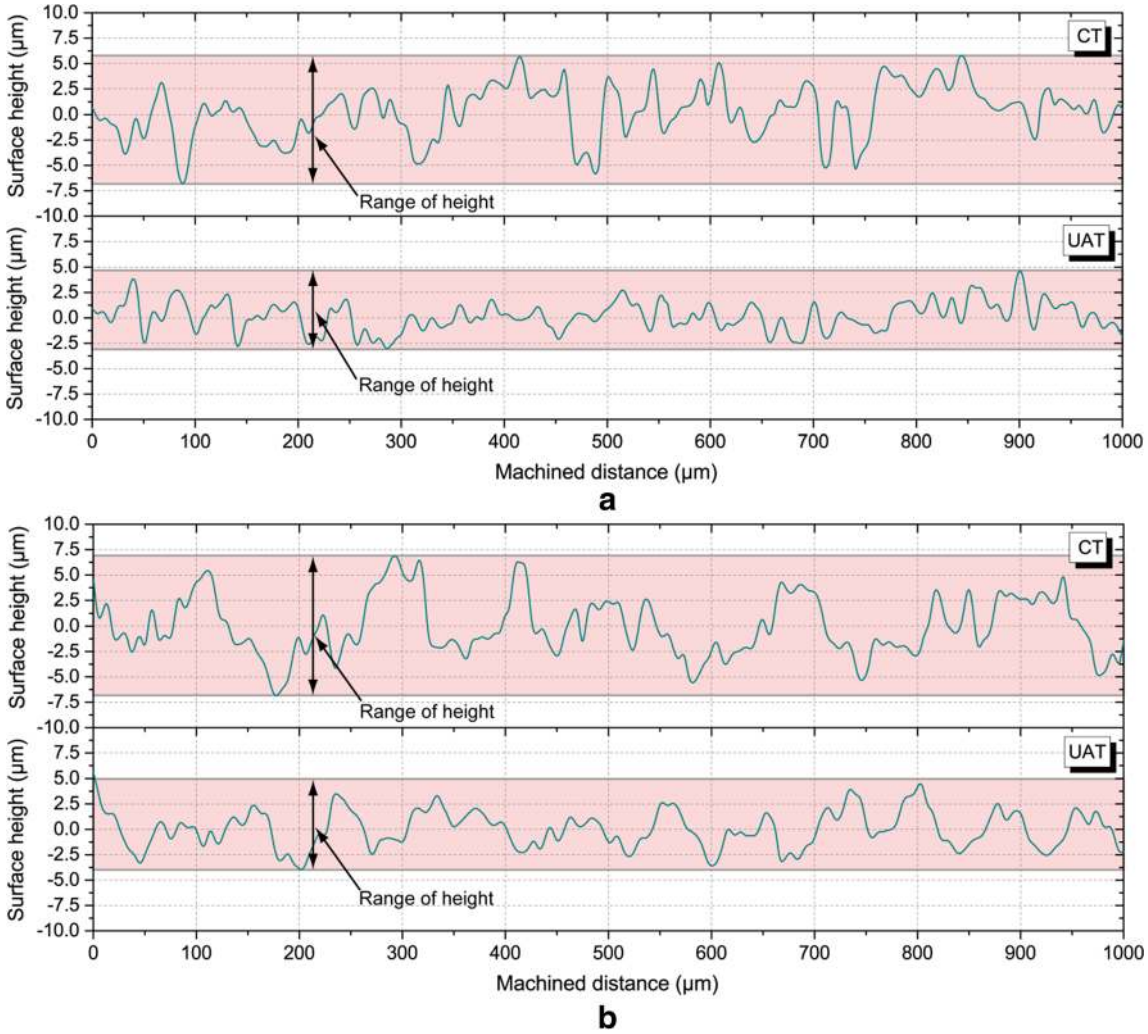

Fig. 6 Surface profiles for machined surfaces in feed direction for CT and UAT: **a** Inconel 718, **b** Inconel 625

profiles were smoother in UAT for both alloys (Fig. 6). The variation in height of the profiles was noticeably lower in UAT when compared to the case of CT of both alloys. Besides, the surface profiles demonstrated that the groove spacing was wider and their heights were higher in Inconel 625 (Fig. 6b) than in Inconel 718 (Fig. 6a), as discussed in the assessment of surface topography (Fig. 5). This phenomenon was validated by magnitudes of surface roughness in Fig. 7(a1, a2): R_a and R_q were higher for Inconel 625 for 20 m/min than those of Inconel 718.

These two well-known surface topography parameters R_a and R_q that represent the arithmetical mean deviation and root mean square of the assessed profiles, respectively, are studied in deatail here. Comparisons of R_a and R_q for both CT and UAT performed with different machining parameters for the two alloys are shown in Fig. 7. Apparently, UAT led to a significant reduction of surface roughness (in terms of R_a and R_q) for two alloys in all the cases. According to the measurements for Inconel 718 (Fig. 7(a1)), surface roughness increased slightly in CT with an increase in the cutting speed from 20 to 40 m/min, and in UAT it increased initially, subsequently decreasing. However, R_a and R_q decreased with the increasing cutting speed for Inconel 625 (Fig. 7(a2)). The reduction of R_a in UAT varied from 34% at 20 m/min to 30% at 30 m/min and 26% at 40 m/min.

The inverse trend for surface roughness with varying cutting speed (Fig. 7(a1, a2)) for the two alloys was probably due to the difference in material and mechanical properties, manifested in the character of the cutting forces (Fig. 3(a1, a2)).

Fig. 7 Comparisons of 2D roughness parameters for various cutting conditions of CT and UAT for Inconel 718 (1) and Inconel 625 (2): (a) varying cutting speed at feed rate of 0.08 mm/rev, depth-of-cut of 0.12 mm, vibration amplitude of 8.4 μm; (b) varying feed rate at cutting speed of 20 m/min, depth-of-cut of 0.12 mm, vibration amplitude of 8.4 μm; (c) varying depth of cut at cutting speed of 20 m/min, feed rate of 0.08 mm/rev, vibration amplitude of 8.4 μm; (d) varying vibration amplitude at cutting speed of 20 m/min, depth-of-cut of 0.12 mm, feed rate of 0.08 mm/rev

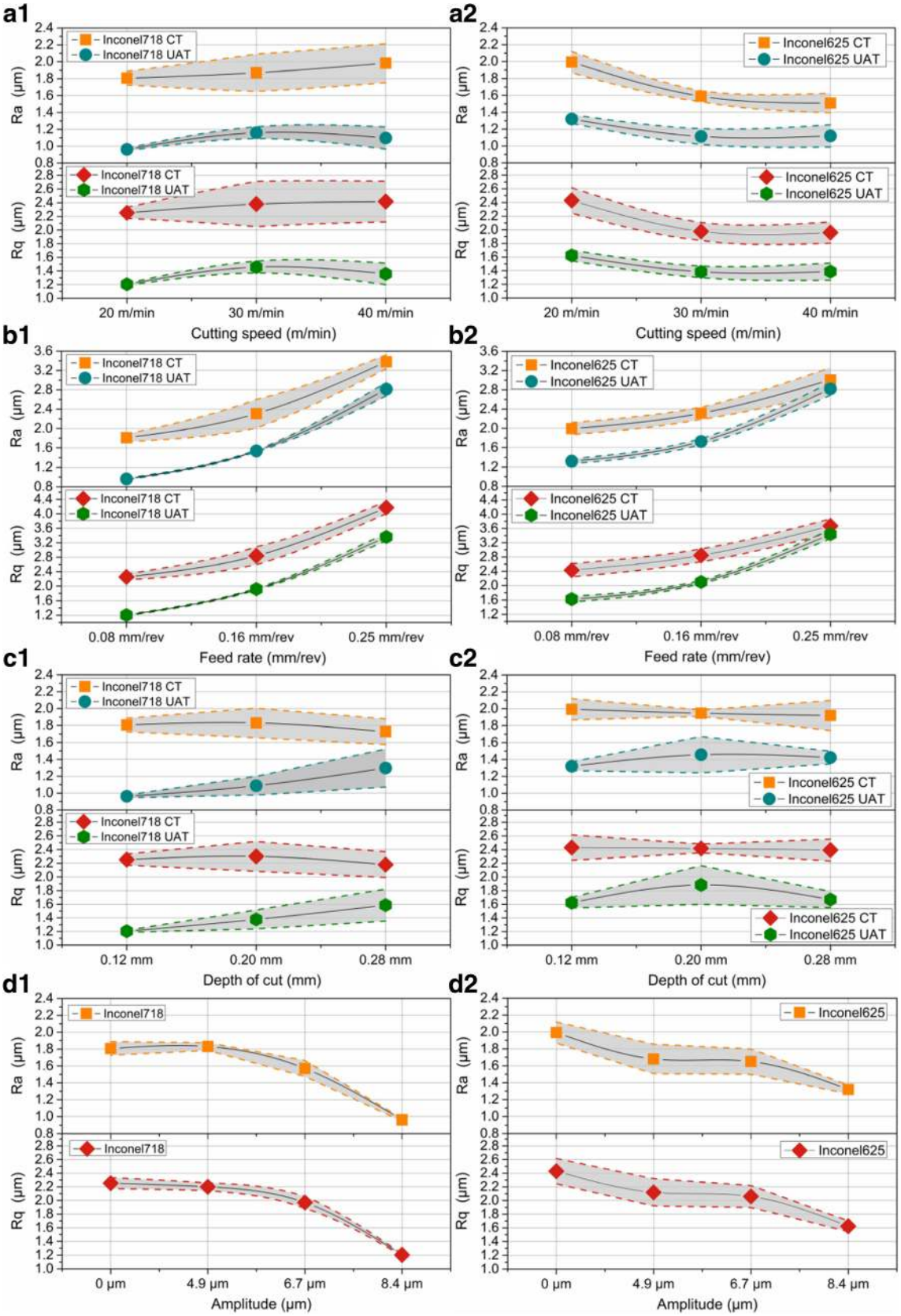
a1
Inconel718 CT
Inconel718 UAT
Ra (μm)
Rq (μm)
20 m/min
30 m/min
40 m/min
Cutting speed (m/min)
a2
Inconel625 CT
Inconel625 UAT
b1
0.08 mm/rev
0.16 mm/rev
0.25 mm/rev
Feed rate (mm/rev)
b2
c1
0.12 mm
0.20 mm
0.28 mm
Depth of cut (mm)
c2
d1
Inconel718
0 μm
4.9 μm
6.7 μm
8.4 μm
Amplitude (μm)
d2
Inconel625

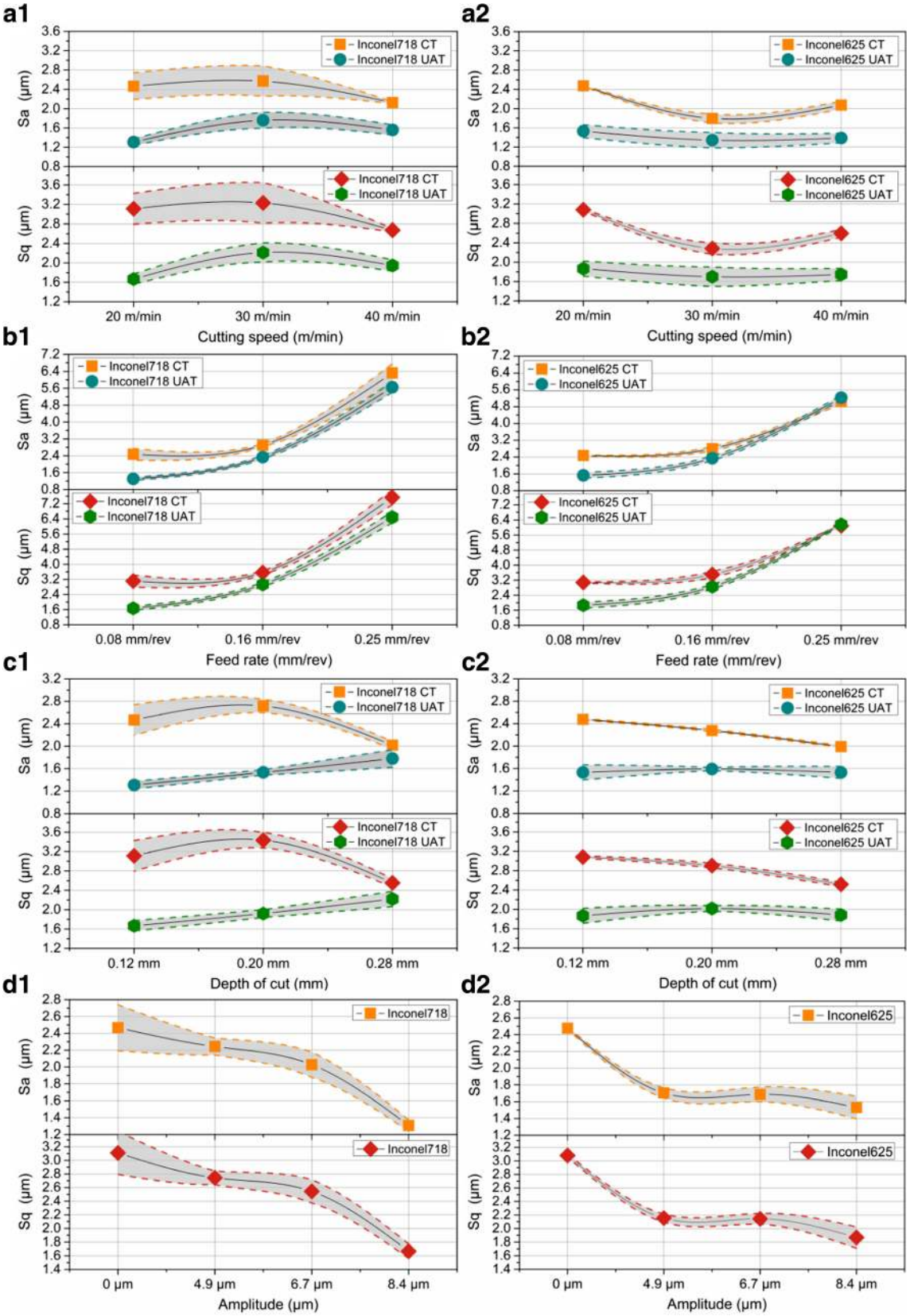
a1
a2
b1
b2
c1
c2
d1
d2
Sa (μm)
Sq (μm)
Inconel718 CT
Inconel718 UAT
Inconel625 CT
Inconel625 UAT
Inconel718
Inconel625
20 m/min
30 m/min
40 m/min
Cutting speed (m/min)
0.08 mm/rev
0.16 mm/rev
0.25 mm/rev
Feed rate (mm/rev)
0.12 mm
0.20 mm
0.28 mm
Depth of cut (mm)
0 μm
4.9 μm
6.7 μm
8.4 μm
Amplitude (μm)

◀ **Fig. 8** Comparisons of 3D roughness parameters for various cutting conditions of CT and UAT for Inconel 718 (1) and Inconel 625 (2): (a) varying cutting speed at feed rate of 0.08 mm/rev, depth-of-cut of 0.12 mm, vibration amplitude of 8.4 μm; (b) varying feed rate at cutting speed of 20 m/min, depth-of-cut of 0.12 mm, vibration amplitude of 8.4 μm; (c) varying depth of cut at cutting speed of 20 m/min, feed rate of 0.08 mm/rev, vibration amplitude of 8.4 μm; (d) varying vibration amplitude at cutting speed of 20 m/min, depth-of-cut of 0.12 mm, feed rate of 0.08 mm/rev

For Inconel 625, R_a and R_q decreased with the increasing cutting speed, as usual for turning most metals. However, the tool wear was significant in turning Inconel 718; thus, the surface roughness increased with cutting speed in CT. The extent of reductions of R_a and R_q in UAT decreased with cutting speed from 20 m/min to 30 m/min, as the cutting speed approached the critical level. When the cutting speed was higher (40 m/min), ultrasonic vibration could still reduce the built-up edge and tool wear although the tool and the workpiece did not separate, reducing the surface roughness.

For a varying feed rate, the magnitudes of R_a and R_q increased significantly for both CT and UAT for the two alloys (Fig. 7(b1, b2)). In addition, the reduction of R_a for Inconel 718 with ultrasonic vibration decreased from 47% at 0.08 mm/rev to 34% at 0.16 mm/rev, followed by 17% at 0.25 mm/rev (Fig. 7(b1)). A similar trend was observed in R_q for Inconel 718 and both R_a and R_q for Inconel 625. This was due to the fact that a lower feed rate implied a shorter travel of the tool in the feed direction, reducing the height of tool tracks decreasing surface roughness. Also, in UAT, due to spurious lateral vibrations, the surface essentially underwent a polishing process, greatly reducing the surface roughness parameters.

Both R_a and R_q in CT demonstrated a non-linear trend with the increasing depth-of-cut for Inconel 718 (Fig. 7(c1)). Other researchers also reported this phenomena [23]. Such a non-linear trend was amplified for S_a and S_q (Fig. 8(c1)). A change in the depth-of-cut did not affect the level of surface roughness significantly for Inconel 625 in CT (Fig. 7(c1, c2)). The reason for this was that the tool wore faster when turning Inconel 718 than Inconel 625. As the depth-of-cut grew for Inconel 718 in CT (Fig. 7(c1)), the increased cutting force and temperature destabilised the cutting process, and the resulted surface quality degraded. At higher magnitudes of the depth-of-cut – 0.28 mm (still, far smaller than the nose radius), severe tool wear led to a decreased effective depth-of-cut, resulting in the decline of surface roughness.

However, for UAT, a larger depth-of-cut led to higher surface roughness for Inconel 718 (Fig. 7(c1)). Thus, the reduction of R_a for machining with ultrasonic assistance reduced from 47% at 0.12 mm to 41% at 0.2 mm and 25% at 0.28 mm. The respective reductions of R_q were 47%, 40% and 27%. This was due to the reduction of the ultrasonic effect on tool wear with a higher depth-of-cut. The surface roughness changed insignificantly in UAT with the increasing depth-of-cut for Inconel 625 (Fig. 7(c2)).

In UAT, for a varying vibration amplitude, comparisons of R_a and R_q are shown in Fig. 7(d1, d2), where the vibration amplitude at 0 μm represents the CT process. It is evident that the larger amplitude led to a greater reduction of surface roughness for both Inconel 718 and 625.

Additionally, 3D roughness parameters S_a and S_q were studied (Fig. 8). The parameters represent, respectively, the average roughness and root mean square roughness evaluated over a representative area on the 3D surface. With the varying feed rate and vibration amplitude, S_a and S_q exhibited similar trends to those of R_a and R_q for the two alloys. The non-linear trends of the 3D roughness parameters were amplified when varying the cutting speed and depth-of-cut in CT. However, in UAT, the trends of S_a and S_q parameters almost the same as for R_a and R_q for two alloys.

3.3 Residual stress

To assess the structural integrity of machined parts, it is essential to characterise the level of residual stresses generated in the component. Here, residual stresses were measured using the XRD technique; the two sets of machining parameters (low and high values) were selected with a cutting speed of 20 m/min and 40 m/min, a feed rate of 0.08 m/min and 0.25 m/min, a depth-of-cut of 0.12 mm and 0.28 mm to show more obvious trends. The uniaxial residual stress of each set was calculated with Eq. (2) and results are summarised in Fig. 9.

Tensile residual stresses were generated in both CT and UAT of Inconel 718 and 625. In UAT, the magnitude of tensile residual stresses was less than that in the samples machined in CT. At cutting speed of 20 m/min, feed rate of 0.08 mm/rev and depth-of-cut of 0.12 mm, the tensile residual stress of + 769.7 MPa in Inconel 718 and + 717.2 MPa in Inconel 625 were measured for CT. The application of ultrasonic vibration (amplitude of 8.4 μm) resulted in lower tensile residual stresses of + 435.9 MPa and + 412.7 MPa, respectively. This clearly demonstrates the benefits for improving fatigue resistance of parts machined with UAT. The microchipping action of the cutting tool in UAT induced a compressive residual stress that helped to compensate some of the tensile residual stress generated by machining. Additionally, generation of spurious vibrations in the radial and feed directions with low amplitudes (~ 1 μm) was unavoidable. Mechanical impacts in the radial direction inevitably led to generation of some compressive residual stress (akin to a shot-peening process). Consequently, a lower tensile residual stress was measured on surfaces machined in UAT.

A reduction of tensile residual stresses was obtained with an increase in the cutting speed in CT (Fig. 9(a1, a2)). It is known that thermal loads lead to tensile residual stresses, whereas mechanical loads results in compressive residual stress [24]. At higher cutting speed, less heat accumulation in shear zone induced lower tensile residual

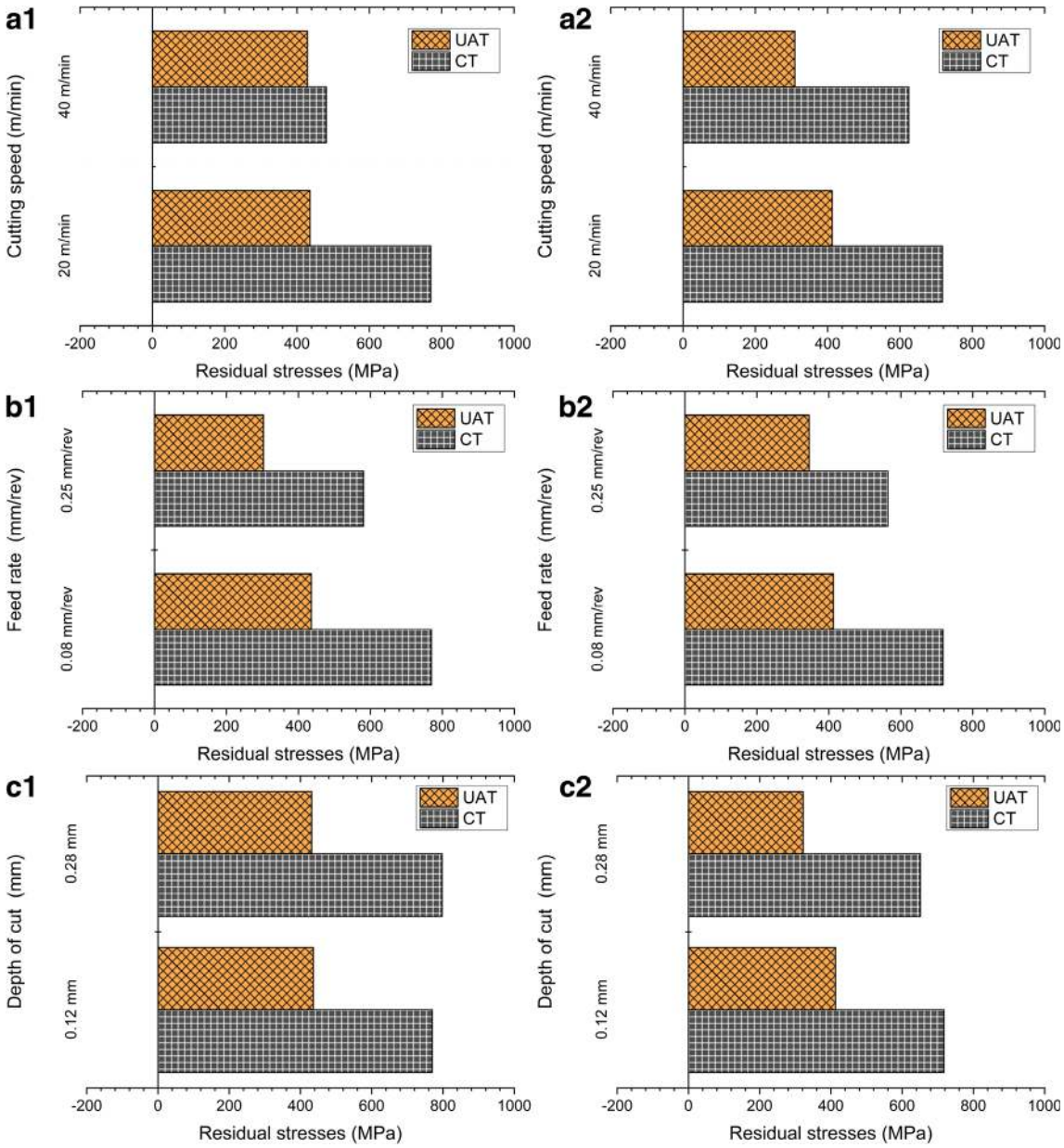

Fig. 9 Residual stresses of machined surface for various cutting conditions of CT and UAT for Inconel 718 (1) and Inconel 625 (2): (a) varying cutting speed at feed rate of 0.08 mm/rev, depth-of-cut of 0.12 mm, vibration amplitude of 8.4 μm; (b) varying feed rate at cutting speed of 20 m/min, depth-of-cut of 0.12 mm, vibration amplitude of 8.4 μm; (c) varying depth of cut at cutting speed of 20 m/min, feed rate of 0.08 mm/rev, vibration amplitude of 8.4 μm

stresses for two alloys in CT. However, lower thermal conductivity of Inconel 625 resulted in more heat accumulation than in Inconel 718, resulting in higher tensile residual stresses at higher cutting speeds. In UAT, the effect of cutting speed on the increase in residual stress was much reduced in Inconel 625 (Fig. 9(a2)) and almost negligible for Inconel 718 (Fig. 9(a1)). It was caused by severe tool wear of Inconel 718, diminishing the reduction of residual stress.

A decline of surface residual stresses with the feed rate in both CT and UAT for two alloys is shown in Fig. 9(b1, b2). A higher feed rate led to a higher cutting force (Fig. 3(b1, b2)); thus, mechanical loading of the tool on the workpiece generated higher compressive residual stresses. The trends of residual stress with the feed rate and reduction of residual stresses in UAT were similar for the two alloys, consistent with the results for the cutting force in Fig. 3(b1, b2).

Figure 9(c1) shows that no visible changes of residual stresses occurred with a varying depth-of-cut in both CT and UAT for Inconel 718, as observed in several studies for other materials [25, 26]. Tensile residual stresses were reduced in both CT and UAT for Inconel 625, which correlated to the

measured cutting forces (Fig. 3(c1, c2)). Higher elongation of Inconel 625 generated larger springback of the surface material; thus, a stress release led to lower residual stresses.

4 Conclusions

A study of the effect of a hybrid machining technique with ultrasonic vibration assistance on machinability and structural integrity of Inconel 718 and 625 was performed with various machining parameters. In this study, noticeable improvements in machinability of two Inconel alloys were achieved using UAT. The possible reasons of reduction of cutting forces, improvements of surface roughness and decline of tensile stresses were assessed and explained. Our study revealed the effects of different materials, mechanical properties and wear behaviours on machinability of two alloys in CT and UAT. The main conclusions of the study are as follows:

1) An appropriate choice of machining parameters, with a cutting speed below the critical magnitude, low levels of feed rate and depth-of-cut along with a higher vibration amplitude can reduce the cutting force significantly in UAT for the studied Inconel alloys.
2) More rapid tool wear of Inconel 718 and higher elongation and lower tensile/shear strength of Inconel 625 led to different changes in cutting force at higher cutting parameters.
3) UAT improved surface topography considerably for various machining parameters for the two studied Inconel alloys. This improvement in UAT decreased with an increase in the feed rate and with the magnitude of the imposed ultrasonic vibration amplitude.
4) The higher elongation of Inconel 625 resulted in higher lateral flow of the machined workpiece material, resulting in larger spacings between grooves and higher heights of surface profile than those of Inconel 718.
5) A study of the machining-induced residual stress showed that in UAT more compressive stresses were generated, helping to reduce the net tensile stresses, which were otherwise generated in (conventional) machining.

Funding information This work was supported by the National Basic Research Program of China (973 Program) grant No. 2013CB035805. This work received financial support from the China Scholarship Council. This work also received funding from the Engineering and Physical Sciences Research Council (UK) through grant EP/K028316/1 and Department of Science and Technology (India) through grant DST/RC-UK/14-AM/2012 for project "Modeling of Advanced Materials for Simulation of Transformative Manufacturing Processes (MAST)" which supported the research performed in UK and India.

References

1. Thakur D, Ramamoorthy B, Vijayaraghavan L (2009) Study on the machinability characteristics of superalloy Inconel 718 during high speed turning. Mater Design 30:1718–1725. https://doi.org/10.1016/j.matdes.2008.07.011
2. Ezugwu E, Bonney J, Yamane Y (2003) An overview of the machinability of aeroengine alloys. J Mater Process Technol 134:233–253. https://doi.org/10.1016/S0924-0136(02)01042-7
3. Sharman ARC, Hughes JI, Ridgway K (2006) An analysis of the residual stresses generated in Inconel 718™ when turning. J Mater Process Technol 173:359–367. https://doi.org/10.1016/j.jmatprotec.2005.12.007
4. Outeiro J, Dias A, Lebrun J (2004) Experimental assessment of temperature distribution in three-dimensional cutting process. Mach Sci Technol 8:357–376. https://doi.org/10.1081/MST-200038984
5. Wardany T, Kishawy H, Elbestawi M (2000) Surface integrity of die material in high speed machining, part 2: microhardness variations and residual stress. J Manuf Sci Eng–T ASME 122:632–641
6. Noyan IC, Cohen JB (2013) Residual stress: measurement by diffraction and interpretation. Springer, Berlin
7. Pawade R, Joshi SS, Brahmankar P (2008) Effect of machining parameters and cutting edge geometry on surface integrity of high-speed turned Inconel 718. Int J Mach Tools Manuf 48:15–28. https://doi.org/10.1016/j.ijmachtools.2007.08.004
8. Arunachalam R, Mannan M, Spowage A (2004) Residual stress and surface roughness when facing age hardened Inconel 718 with CBN and ceramic cutting tools. Int J Mach Tools Manuf 44:879–887. https://doi.org/10.1016/j.ijmachtools.2004.02.016
9. Dudzinski D, Devillez A, Moufki A, Larrouquere D, Zerrouki V, Vigneau J (2004) A review of developments towards dry and high speed machining of Inconel 718 alloy. Int J Mach Tools Manuf 44:439–456. https://doi.org/10.1016/S0890-6955(03)00159-7
10. Maurotto A, Muhammad R, Roy A, Silberschmidt VV (2013) Enhanced ultrasonically assisted turning of a β-titanium alloy. Ultrasonics 53:1242–1250. https://doi.org/10.1016/j.ultras.2013.03.006
11. Babitsky V, Mitrofanov A, Silberschmidt VV (2004) Ultrasonically assisted turning of aviation materials: simulations and experimental study. Ultrasonics 42:81–86. https://doi.org/10.1016/j.ultras.2004.02.001
12. Mitrofanov A, Ahmed N, Babitsky V, Silberschmidt VV (2005) Effect of lubrication and cutting parameters on ultrasonically assisted turning of Inconel 718. J Mater Process Technol 162:649–654. https://doi.org/10.1016/j.jmatprotec.2005.02.170
13. Nath C, Rahman M (2008) Effect of machining parameters in ultrasonic vibration cutting. Int J Mach Tools Manuf 48:965–974. https://doi.org/10.1016/j.ijmachtools.2008.01.013
14. Nath C, Rahman M, Neo KS (2009) Machinability study of tungsten carbide using PCD tools under ultrasonic elliptical vibration cutting. Int J Mach Tools Manuf 49:1089–1095. https://doi.org/10.1016/j.ijmachtools.2009.07.006

15. Sharma V, Pandey PM (2016) Optimization of machining and vibration parameters for residual stresses minimization in ultrasonic assisted turning of 4340 hardened steel. Ultrasonics 70:172–182. https://doi.org/10.1016/j.ultras.2016.05.001
16. Nestler A, Schubert A (2014) Surface properties in ultrasonic vibration assisted turning of particle reinforced aluminium matrix composites. Procedia CIRP 13:125–130. https://doi.org/10.1016/j.procir.2014.04.022
17. Ahmed N, Mitrofanov A, Babitsky V, Silberschmidt VV (2006) Analysis of material response to ultrasonic vibration loading in turning Inconel 718. Mater Sci Eng A-Struct 424:318–325. https://doi.org/10.1016/j.msea.2006.03.025
18. Bai W, Sun RL, Leopold J, Silberschmidt VV (2017) Microstructural evolution of Ti6Al4V in ultrasonically assisted cutting: numerical modelling and experimental analysis. Ultrasonics 78:70–82. https://doi.org/10.1016/j.ultras.2017.03.005
19. Lu J (1996) Handbook of measurement of residual stresses. Fairmont Press
20. Prevéy PS (1996) Current applications of X-ray diffraction residual stress measurement. Dev Mater Charact Technol:103–110
21. Devillez A, Schneider F, Dominiak S, Dudzinski D, Larrouquere D (2007) Cutting forces and wear in dry machining of Inconel 718 with coated carbide tools. Wear 262:931–942. https://doi.org/10.1016/j.wear.2006.10.009
22. Liao YS, Shiue RH (1996) Carbide tool wear mechanism in turning of Inconel 718 superalloy. Wear 193:16–24. https://doi.org/10.1016/0043-1648(95)06644-6
23. Lalwani D, Mehta N, Jain P (2008) Experimental investigations of cutting parameters influence on cutting forces and surface roughness in finish hard turning of MDN250 steel. J Mater Process Technol 206:167–179. https://doi.org/10.1016/j.jmatprotec.2007.12.018
24. Halverstadt R (1959) How to minimize and control residual machining stresses. Am Mach 103:138
25. Dahlman P, Gunnberg F, Jacobson M (2004) The influence of rake angle, cutting feed and cutting depth on residual stresses in hard turning. J Mater Process Technol 147:181–184. https://doi.org/10.1016/j.jmatprotec.2003.12.014
26. Capello E (2005) Residual stresses in turning: part I: influence of process parameters. J Mater Process Technol 160:221–228. https://doi.org/10.1016/j.jmatprotec.2004.06.012